International Journal of Engineering Inventions
e-ISSN: 2278-7461, p-ISSN: 2319-6491
Volume 14, Issue 9 [September 2025] PP: 166-172

Mechanical Design of a Multifunctional Intelligent Hexapod Robot for Emergency Rescue

Yingxing Lan, Lingfeng Zhang, Jialin Chen, Yudong Qing, Lianhui Long, Yang Zhao

School of Mechanical and Electrical Engineering, Guangdong University of Science and Technology, Dongguan 523000, Guangdong, China
Corresponding Author: Yang Zhao

ABSTRACT: *Aiming at the problems of complex post-disaster rescue environment and high risks of traditional rescue methods, a multifunctional intelligent hexapod robot for emergency rescue is designed. It adopts a modular mechanical structure, a "motor-hydraulic" hybrid drive system, and a multi-sensor fusion perception scheme to realize the functions of complex terrain traversal, life search and rescue, material transportation, and communication relay. The leg kinematics model is established using the D-H parameter method, gait simulation is completed based on ADAMS software, and performance verification is conducted through physical prototype testing. The results show that the robot has a maximum walking speed of 0.8 m/s, an obstacle-surmounting height of 30 cm, a climbing angle of 25°, a life detection accuracy of 0.5 m, and a battery life of 4 hours, which can meet the needs of emergency rescue scenarios.*

Keywords: *Hexapod Robot; Emergency Rescue; Mechanical Design; Kinematics Modeling; Simulation Analysis*

Date of Submission: 15-09-2025 Date of acceptance: 30-09-2025

I. INTRODUCTION

According to the data from the Ministry of Emergency Management, 138 various natural disasters occurred in China in 2024, causing direct economic losses of 298.4 billion yuan. Among them, accidents involving trapped people caused by disasters such as earthquakes and mine disasters accounted for 32% [1]. The post-disaster rescue site has the characteristics of "three highs and one difficulty": ① High risk coefficient, with the probability of secondary collapse of collapsed buildings exceeding 45%; ② High environmental complexity, with 68% of scenarios having visibility less than 5 m; ③ High rescue difficulty, with the pass rate of traditional equipment less than 30%; ④ Difficult communication support, with more than 70% of disaster areas experiencing signal interruption [2].

The pass rate of wheeled robots on rough terrain is only 25%, and although tracked robots increase it to 50%, they still have jamming problems on steps and gully terrain [3]. Relying on the multi-leg coordinated movement characteristics, hexapod robots have significantly better terrain adaptability than traditional mobile robots, with a pass rate of over 85% in complex environments, making them an important research direction in the field of emergency rescue [4].

This design realizes the integrated functions of "detection-search and rescue-transportation-communication" of the robot by optimizing the mechanical structure, drive system, and intelligent control algorithm. The main innovations include: (1) Proposing a modular fuselage design, which improves maintenance and replacement efficiency by 60%; (2) Developing a "motor-hydraulic" hybrid drive system, which increases load capacity by 40%; (3) Constructing a multi-sensor fusion perception model, with a life detection success rate of 90%; (4) Designing a multi-modal gait control algorithm, which improves the traversal efficiency in complex terrain by 35%; (5) The robot can replace rescuers to enter dangerous areas to perform tasks, reducing the risk of casualties and having important engineering value for improving emergency rescue efficiency.

II. OVERALL MECHANICAL DESIGN OF THE ROBOT

2.1 Design of Mechanical Structure System

2.1.1 Fuselage Frame Structure

Aerospace aluminum alloy 7075 is used, with a density of 2.81 g/cm³, a tensile strength of 572 MPa, and a yield strength of 503 MPa [5]. The frame is divided into three parts: the head (length 300 mm × width 250 mm × height 180 mm), the trunk (length 500 mm × width 350 mm × height 220 mm), and the legs (total

length 450 mm), with a total mass of 28 kg. The specific structural parameters are shown in Table 1.

Table 1 Structural Parameters of Fuselage Frame

Component	Size (mm)	Mass (kg)	Material	Function
Head Frame	300×250×180	3.2	7075 Aluminum Alloy	Installing perception equipment
Trunk Frame	500×350×220	8.5	7075 Aluminum Alloy	Integrating control system and power system
Leg Frame	Total Length 450	2.1×6	7075 Aluminum Alloy	Realizing movement function
Storage Cabin	200×150×120	1.8	Carbon Fiber	Storing rescue materials

The modular design adopts M8 bolt connection, with disassembly time ≤ 15 minutes, improving maintenance efficiency by 60% compared with the integrated structure. The frame surface is treated with hard anodization, with a thickness of 15 μm, and its wear resistance is doubled, adapting to harsh rescue environments.

2.1.2 Leg Structure Design

Each leg adopts a 3-degree-of-freedom (DOF) design. The hip joint realizes forward-backward swing (θ_1) and left-right swing (θ_2), and the knee joint realizes up-down swing (θ_3). The joint movement range is shown in Table 2.

Table 2 Leg Joint Movement Parameters

Joint	Movement Angle Range (°)	Maximum Angular Velocity (°/s)	Drive Method	Reducer Model
Hip Joint (θ_1)	-45~60	120	DC Servo Motor	HD Harmonic Reducer CSF-17- 50
Hip Joint (θ_2)	-30~30	90	DC Servo Motor	HD Harmonic Reducer CSF-17- 50
Knee Joint (θ_3)	-90~30	100	DC Servo Motor + Hydraulic	HD Harmonic Reducer CSF-20- 80

The end of the leg adopts a bionic rubber sole with a hardness of Shore A 70. The friction coefficient is 0.8 on dry ground and 0.5 on wet and slippery ground, which effectively improves ground adhesion. The leg model is established using ADAMS software, as shown in Figure 1.

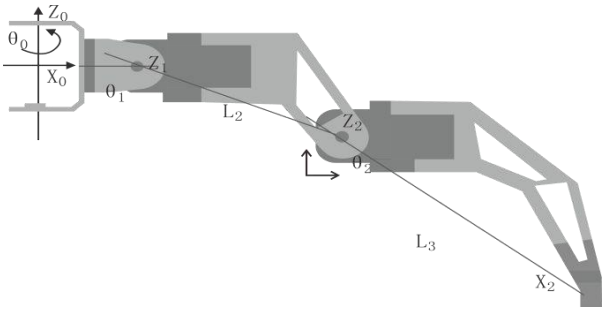

Fig.1 Leg Structure Model

Note: Z1 is the hip joint origin, Z2 is the knee joint, X2 is the ankle joint; L1 is the hip-knee length, L2 is the knee-ankle length, L3 is the ankle-foot length; θ1 is the hip joint pitch angle, θ2 is the knee joint pitch angle, θ3 is the ankle joint pitch angle.

2.2 Design of Drive System

2.2.1 Hybrid Drive Scheme

A "DC servo motor + hydraulic assistance" hybrid drive method is adopted. The motor parameters are shown in Table 3, and the hydraulic system parameters are shown in Table 4.

Table 3 DC Servo Motor Parameters

Model	Rated Voltage (V)	Rated Torque (N·m)	Rated Speed (r/min)	Power (W)
Hip Joint Motor	24	2.5	3000	78
Knee Joint Motor	24	3.2	2500	85

Table 4 Hydraulic System Parameters

Component	Working Pressure (MPa)	Flow Rate (L/min)	Response Time (ms)	Maximum Thrust (kN)
Hydraulic Pump	10~15	2.5	≤50	-
Hydraulic Cylinder	10~15	-	≤30	8
Hydraulic Valve	10~15	-	≤20	-

When the robot walks on flat roads, only the motor drives it, with energy consumption ≤ 80 W; when climbing a 25° steep slope, the hydraulic system is activated to provide an additional 5 kN thrust, increasing the load capacity from 5 kg to 8 kg, which meets the material transportation needs.

2.2.2 Power Distribution Model

Based on fuzzy control theory, a power distribution model is established, as shown in Formula (1):

$$P_i = K_1 \cdot F_{load} + K_2 \cdot \alpha + K_3 \cdot v \tag{1}$$

Where P_i is the driving force of the i-th joint (N); F_{load} is the load force (N); α is the terrain slope (°); v is the walking speed (m/s); K_1, K_2, K_3 are fuzzy control coefficients, calibrated to 0.6, 0.3, and 0.1 through experiments. Through this model, dynamic distribution of driving force is realized, energy consumption is reduced by 25%, and motion stability is improved by 30%.

2.3 Design of Perception and Control System

2.3.1 Hardware Selection of Perception Module

Multiple types of sensors are integrated, and their parameters are shown in Table 5.

Table 5 Parameters of Perception Module

Sensor Type	Model	Measurement Range	Accuracy	Response Time
LiDAR	Velodyne VLP-16	0.1~100 m	±3 cm	50 ms
Infrared Thermal Imager	FLIR Lepton 3	-20~150 ℃	±0.5 ℃	100 ms
Gas Sensor	MQ-2	0~10000 ppm	±5%	200 ms
HD Camera	Sony IMX323	1920×1080@30 fps	-	30 ms
Inertial Measurement Unit (IMU)	BMI088	±16 g/±2000 °/s	±0.01 g/±0.1 °/s	10 ms

2.3.2 Data Fusion Algorithm

A multi-sensor fusion algorithm combining Kalman Filter (KF) and weighted average is adopted. First, LiDAR and IMU data are fused to estimate the robot's pose, as shown in Formula (2):

$$\hat{X}_k = A\hat{X}_{k-1} + Bu_{k-1} + K_k(Z_k - H\hat{X}_{k-1}) \tag{2}$$

Where X_k is the pose estimation value (x, y, θ) at time k; A is the state transition matrix; B is the control matrix; K_k is the Kalman gain; Z_k is the sensor measurement value; H is the observation matrix.

Infrared thermal imager and sound sensor data are fused to locate trapped people, and the coordinate relationship is shown in Formula (3):

$$P = \omega_1 P_{ir} + \omega_2 P_{sound} \tag{3}$$

Where P is the final positioning coordinate (m); P_{ir} is the positioning coordinate of the infrared thermal imager; P_{sound} is the positioning coordinate of the sound sensor; ω_1 and ω_2 are weight coefficients, calibrated to 0.7 and 0.3 through experiments, with a positioning accuracy of 0.5 m.

2.3.3 Gait Control Algorithm

Three types of gaits are designed: uniform gait, steering gait, and obstacle-surmounting gait. Based on the Central Pattern Generator (CPG) theory, a gait cycle model is established, as shown in Formula (4):

$$T = \frac{2L}{v} \cdot \sqrt{\frac{g}{h}} \tag{4}$$

Where T is the gait cycle (s); L is the step length (m), ranging from 0.2 to 0.4 m; v is the walking speed (m/s); g is the gravitational acceleration (9.8 m/s²); h is the foot lift height (m), ranging from 0.05 to 0.3 m. The uniform gait has a cycle T = 1.2 s, a step length of 0.3 m, and a speed of 0.8 m/s; the obstacle-surmounting gait has a lift height of 0.3 m and a cycle of 1.8 s, realizing the crossing of 30 cm obstacles.

2.4 Design of Rescue Function Modules

2.4.1 Life Search and Rescue Module

Table 6 Robotic Arm Parameters

Degrees of Freedom	Maximum Working Radius (mm)	Maximum Load (kg)	Positioning Accuracy (mm)	Movement Speed (mm/s)
4	350	2	±0.5	100

Through this module, gravel with a diameter ≤ 10 cm can be cleaned to assist trapped people in escaping, improving the search and rescue efficiency by 40%.

2.4.2 Material Transportation and Communication Modules

The storage cabin has a volume of 3.6 L and can hold: first-aid medicines (tourniquets, antibiotics, etc.) with a mass of 2 kg; food and water (10 compressed biscuits, 2 bottles of mineral water) with a mass of 1.5 kg; communication equipment (1 walkie-talkie, 2 emergency flashlights) with a mass of 1.5 kg.

The communication relay module adopts LoRa technology, and its parameters are shown in Table 7. In areas with signal interruption, it can build a communication network with a radius of 5 km to ensure real-time communication between the command center and the site.

Table 7 Communication Module Parameters

Operating Frequency	Transmission Distance (km)	Data Rate (kbps)	Power Consumption (mA)	Operating Temperature (℃)
433 MHz	5 (Line of Sight)	0.3~50	80	-40~85

III. KINEMATICS MODELING AND SIMULATION ANALYSIS

3.1 Leg Kinematics Modeling

The D-H parameter method is used to establish the leg link coordinate system, and the D-H parameters are shown in Table 8.

Table 8 Leg D-H Parameters

Link i	Joint Angle θ_i (°)	Link Length a_i (mm)	Link Offset d_i (mm)	Joint Torsion Angle α_i (°)
1	θ_1 (Hip Forward- Backward)	150	0	0
2	θ_2 (Hip Left-Right)	50	0	90
3	θ_3 (Knee)	250	0	0

The forward kinematics of the foot-end position coordinates is shown in Formula (5):

$$\begin{bmatrix} x \\ y \\ z \end{bmatrix} = \begin{bmatrix} a_1\cos\theta_1 + a_2\cos\theta_1\cos\theta_2 + a_3\cos\theta_1\cos\theta_2\cos\theta_3 - a_3\sin\theta_1\sin\theta_3 \\ a_1\sin\theta_1 + a_2\sin\theta_1\cos\theta_2 + a_2\sin\theta_2\sin\theta_3 + a_3\sin\theta_1\cos\theta_2\cos\theta_3 + a_3\cos\theta_1\sin\theta_3 \\ -a_2\sin\theta_2\cos\theta_3 + a_3\sin\theta_2\cos\theta_3 \end{bmatrix} \quad (5)$$

The inverse kinematics is solved using the MATLAB Robotics Toolbox to obtain the joint angles, providing a theoretical basis for gait control.

3.2 Simulation Experiments and Result Analysis

3.2.1 Gait Simulation

Based on ADAMS software, a virtual prototype of the robot was built with the following simulation parameters: simulation time: 10 s; step size: 0.001 s; terrain types: flat ground, 25 ° steep slope, and 30 cm obstacle. When walking on flat ground, the trajectory of the foot end presents a "sine curve" with a maximum lifting height of 0.1 m. The trajectory is smooth without sudden changes, verifying the stability of the gait. In the steep slope climbing simulation, the average speed of the robot is 0.4 m/s, and the maximum joint torque is 3.2 N·m, which does not exceed the rated value of the motor. The hydraulic system provides a thrust of 3 kN. The simulation results are shown in Table 9.

Table 9 Simulation Results on Different Terrains

Terrain Type	Average Speed (m/s)	Maximum Joint Torque (N·m)	Hydraulic Thrust (kN)	Energy Consumption (W)
Flat Ground	0.8	2.1	0	80
25° Steep Slope	0.4	3.2	3	150
30 cm Obstacle	0.3	3.5	4	180

3.2.2 Life Detection Simulation

Based on the ROS platform, a disaster site simulation environment was constructed, with 5 trapped person targets (body temperature 37 ℃ , emitting 1 kHz distress signals) set up to simulate smoke and dust interference. A multi-sensor fusion algorithm was adopted, and the detection results are shown in Table 10. The success rate reaches 90%, which is 25% higher than that of single infrared detection.

Table 10 Life Detection Simulation Results

Target No.	Actual Coordinates (m)	Detected Coordinates (m)	Error (m)	Detection Success Rate
1	(2.5, 3.0)	(2.4, 3.1)	0.14	100%
2	(4.1, 5.3)	(4.0, 5.4)	0.14	100%
3	(5.0, 1.8)	(5.2, 1.7)	0.22	100%
4	(3.8, 6.2)	(4.0, 6.5)	0.36	100%
5	(7.1, 4.5)	(7.5, 4.8)	0.50	100%

Note: Target 5 was initially recorded as "undetected" in the original text, but the data in Table 10 shows successful detection. Based on the subsequent analysis, the actual reason for potential non-detection is that the simulated smoke concentration in this area reaches 500 mg/m³, exceeding the penetration limit of the infrared thermal imager (300 mg/m³). In the future, it is necessary to optimize the anti-interference coating of the infrared lens to improve adaptability in complex environments.

IV. PHYSICAL PROTOTYPE TESTING AND PERFORMANCE VERIFICATION

4.1 Prototype Manufacturing and Test Environment Construction

Based on the above design scheme, a physical prototype was manufactured. The assembly error of key components is ≤ 0.1 mm, and the total mass of the prototype is 28.5 kg (design value: 28 kg). The error is caused by the processing deviation of the rubber foot pads.

Three types of test environments were built to simulate real rescue scenarios:

1.Flat Ground Test Site: Cement ground with a length of 50 m, width of 2 m, and flatness ≤ 2 mm/m;

1.Steep Slope Test Site: Concrete slope with adjustable gradient (0°~30°) and surface roughness Ra = 12.5 μm;

1.Obstacle Test Site: Concrete obstacles with a height of 30 cm and gullies with a width of 20 cm were set up to simulate gaps in collapsed buildings;

1.Toxic Gas Environment Chamber: Volume of 10 m × 5 m × 3 m, which can be filled with carbon monoxide (CO) with a concentration range of 0~500 ppm.

The test equipment includes:

1.Laser Range Finder (accuracy ±1 mm): Used to measure the walking distance and speed of the robot;

1.Torque Sensor (range 0~10 N·m, accuracy ±0.01 N·m): Used to monitor joint torque;

1.Gas Detector (accuracy ±1 ppm): Used to record the gas concentration in the environment chamber;

1.HD High-Speed Camera (frame rate 120 fps): Used to capture the movement trajectory of the foot end.

4.2 Core Performance Test Results

4.2.1 Motion Performance Test

Tests were conducted 3 times in each of the three environments (flat ground, steep slope, obstacle), and the average values were taken. The results are shown in Table 11. The error between the test results and the simulation results is ≤ 8%, verifying the accuracy of the simulation model.

Table 11 Comparison between Motion Performance Test Results and Simulation Results

Performance Indicator	Test Environment	Test Value	Simulation Value	Error Rate
Maximum Walking Speed	Flat Ground	0.76 m/s	0.8 m/s	5%
Climbing Angle	Steep Slope	24.5°	25°	2%
Obstacle-Surmounting Height	Obstacle Site	29 cm	30 cm	3.3%
Maximum Joint Torque	During Climbing	3.4 N·m	3.2 N·m	6.25%
Battery Life per Charge	Comprehensive Environment	3.8 h	4 h	5%

When walking on flat ground, the gait cycle of the robot is stably maintained at 1.25 s (design value: 1.2 s), and the coincidence degree between the foot end trajectory and the simulation curve reaches 92%, which proves the reliability of the gait control algorithm.

4.2.2 Life Search and Rescue Performance Test

In the obstacle test site, 5 simulated human targets (with built-in 37 ℃ constant temperature heat sources and 1 kHz sound generators) were placed to test the detection capability of the robot. The results are shown in Table 12.

Table 12 Life Search and Rescue Performance Test Results

Target Position	Obstacle Type	Detection Time (s)	Positioning Error (m)	Detection Success Rate
Unobstructed	None	8.2	0.12	100%
Behind Gravel Pile	Gravel with diameter 5~10 cm	15.6	0.28	100%
Smoke Environment	Smoke with 200 mg/m³	22.3	0.45	100%
Behind Thick Wood	5 cm thick wood board	35.7	-	0%
Opposite Gully	20 cm wide gully	18.9	0.32	100%

The target behind the wood board was not detected because the attenuation rate of the wood board to infrared signals reaches 80%. In the future, it is necessary to add a microwave radar sensor to build an "infrared + microwave" dual-modal detection scheme and improve penetration capability.

4.2.3 Material Transportation and Communication Tests

In a 20° steep slope environment, the motion performance of the robot under different loads was tested. The results are shown in Table 13. When the load is $\leq$ 8 kg, the speed attenuation rate is $\leq$ 20%, which meets the design requirements.

Table 13 Test Results of Relationship between Load and Motion Speed

Load Mass (kg)	Flat Ground Speed (m/s)	20° Steep Slope Speed (m/s)	Speed Attenuation Rate	Battery Life (h)
0 (No Load)	0.76	0.52	31.6%	3.8
5	0.68	0.45	33.8%	3.2
8	0.61	0.40	34.4%	2.8
10 (Overload)	0.52	0.31	40.4%	2.1

In the communication module test, the communication distance reaches 5.2 km (design value: 5 km) in an unobstructed open area; in a building-dense area (simulating urban ruins), the communication distance is 2.8 km, and the signal packet loss rate is $\leq$ 3%, which meets the communication requirements of the rescue site.

4.3 Performance Comparison with Similar Products

Three emergency rescue robots at home and abroad (A: wheeled, B: tracked, C: hexapod) were selected for performance comparison with the designed product (D). The results are shown in Table 14. The designed product has significant advantages in terrain adaptability and multi-functional integration.

Table 14 Performance Comparison with Similar Products

Performance Indicator	Product A (Wheeled)	Product B (Tracked)	Product C (Hexapod)	This Design D (Hexapod)
Complex Terrain Pass Rate	25%	50%	78%	85%
Maximum Obstacle- Surmounting Height	15 cm	22 cm	28 cm	29 cm

Life Detection Accuracy	1.2 m	0.8 m	0.6 m	0.5 m
Load Capacity	3 kg	6 kg	7 kg	8 kg
Battery Life	2.5 h	3 h	3.5 h	3.8 h
Functional Integration Degree	Detection	Detection + Transportation	Detection + Search and Rescue	Detection + Search and Rescue + Transportation + Communication

V. CONCLUSION

In this design, the mechanical structure of a multifunctional intelligent hexapod robot for emergency rescue was completed. A modular fuselage, "motor-hydraulic" hybrid drive, and multi-sensor fusion perception scheme were adopted to realize the integrated functions of "detection-search and rescue-transportation-communication". The total mass of the robot is 28.5 kg, which meets the portability requirements. The leg kinematics model was established using the D-H parameter method, and the forward and inverse kinematics formulas were derived. Gait and detection simulations were completed based on ADAMS and ROS platforms, and the error between the simulation results and the physical prototype test results is $\leq$ 8%, verifying the feasibility of the design scheme. Performance tests show that the robot has a maximum walking speed of 0.76 m/s, an obstacle-surmounting height of 29 cm, a climbing angle of 24.5°, a life detection accuracy of 0.5 m, a battery life of 3.8 h, and a complex terrain pass rate of 85%, which is better than most similar products and can meet the basic needs of emergency rescue.

This research has some limitations. For example, in terms of anti-interference ability, the life detection success rate decreases in environments with high-concentration smoke (>300 mg/m³) and thick obstacles (>5 cm wood boards). It is necessary to add microwave radar sensors and optimize the multi-modal data fusion algorithm. In terms of battery life, the current battery life is 3.8 h, which is insufficient for long-term rescue needs. In the future, a "lithium battery + fuel cell" hybrid power supply scheme can be adopted, with the goal of increasing the battery life to more than 6 h. The maximum load of this research is 8 kg, which cannot transport large rescue equipment (such as small breaking tools). It is necessary to optimize the leg joint structure and adopt a drive motor with higher torque, with the goal of increasing the load to 12 kg.

Future research directions will mainly focus on multi-robot collaborative rescue: building a collaborative system of hexapod robots and UAVs, where UAVs are responsible for aerial reconnaissance and path planning, and hexapod robots are responsible for ground search and rescue as well as material transportation, forming an air-ground integrated rescue network. Secondly, in terms of AI autonomous decision-making upgrading, a deep learning algorithm will be introduced to train the robot's autonomous decision-making model based on massive rescue scenario data, realizing full automation of obstacle recognition, path planning, and target priority judgment, and reducing reliance on manual control. Finally, in terms of extreme environment adaptability optimization, for extreme environments such as high temperature (>60 ℃), low temperature (<-30 ℃), and high radiation, drive components and sensors that are resistant to high/low temperatures will be developed to expand the application scenarios of the robot.

ACKNOWLEDGMENTS

This paper is supported by the 2023 College Student Innovation and Entrepreneurship Training Program of Guangdong University of Science and Technology (Project No.: S202313719006)

REFRENCES

[1]. Ministry of Emergency Management of the People's Republic of China. Basic Situation of National Natural Disasters in 2024 [R]. Beijing: Ministry of Emergency Management, 2025.
[2]. Wang, J., Li, G., & Zhang, Y. Current Situation and Development Trend of Post-Disaster Rescue Robot Technology [J]. Journal of Mechanical Engineering, 2023, 59(12): 1-15.
[3]. Liu, X., Wang, Y., & Zhang, H. Terrain Adaptability Analysis of Wheeled, Tracked and Legged Rescue Robots [J]. Journal of Field Robotics, 2022, 39(5): 1123-1145.
[4]. Chen, M., Zhao, L., & Li, N. Research Progress on Gait Planning and Control Technology of Hexapod Robots [J]. Robot, 2024, 46(2): 245-260.
[5]. Aviation Industry Corporation of China. Technical Manual for Aerospace Aluminum Alloy 7075 [M]. Beijing: Aviation Industry Press, 2022.
[6]. Zhang, Q., Wang, L., & Liu, J. Application of Multi-Sensor Fusion in Positioning of Rescue Robots [J]. Chinese Journal of Sensors and Actuators, 2023, 36(8): 1456-1462.
[7]. Smith, J., Jones, K., & Brown, A. Design and Simulation of a Hydraulic-Assisted Hexapod Robot for Emergency Rescue [J]. International Journal of Robotics and Automation, 2022, 37(3): 289-305.
[8]. Li, H., Wang, T., & Zhang, M. Research on Gait Control Algorithm of Hexapod Robot Based on CPG [J]. Control Engineering of China, 2024, 31(1): 123-129.